Supporting Information

Composite Polymer Electrolytes Incorporating Two-Dimensional Metal Organic Frameworks Enables Ultra-Long Cycling Solid-State Lithium Batteries

Han Jiang[a], Meiqi Huang[a], Yongqian Du[a], Jiangrong Kong*[a], Peng Liu[b], Tao Zhou[a]

[a] *Hunan Provincial Key Laboratory of Efficient and Clean Utilization of Manganese Resources, College of Chemistry and Chemical Engineering, Central South University, Changsha, 410083, China*

[b] *School of Materials Science and Engineering, Changsha University of Science and Technology, Changsha 410114, China*

*Corresponding author.

E-mail address: kongjr@csu.edu.cn (J. Kong).

1. Experimental section

1.1. Materials preparation

Cobalt nitrate hexahydrate [$Co(NO_3)_2 \cdot 6H_2O$], terephthalic acid (1,4-H_2BDC), N,N-Dimethylformamide (DMF) and triethylamine (TEA) were purchased from Shanghai Sinopharm Chemical Reagent Co., Ltd. N-Methyl-pyrrolidone (NMP) was purchased from Adamas-beta. Poly (vinylidene fluoride) (PVDF, Mw~1000000), Lithium bis(trifluoromethanesulfonic) imide salt (LiTFSI), $LiFePO_4$ (LFP), Li foils and coin-cell case (CR2016) were purchased from Kelude Materials Technology Co., Ltd. All chemical reagents were Analytical Reagent (AR) and used directly without further purification.

1.2. Preparation of two-dimensional cobalt-based ultrathin metal-organic framework nanosheets (CMS)

2D Co-MOF nanosheets (CMS) were synthesized using $Co(NO_3)_2 \cdot 6H_2O$ and 1,4-H_2BDC by the traditional hydrothermal method. 1 mmol $Co(NO_3)_2 \cdot 6H_2O$ and 1 mmol 1,4-H_2BDC were dissolved in a solution of 30 mL DMF and 2 mL deionized water. Then, 0.6 mL TEA was injected into the solution, which was stirred for 10 min to obtain a uniform colloidal suspension. The mixture was transferred into a 50 mL Teflon-lined stainless steel at 160℃ for 18 h. The products were obtained via centrifugation, washed three times with ethanol, and dried at 80℃ overnight. The obtained CMS was first heated at 80°C for 12 h in vacuum to remove a small amount of absorbed DMF and water from the precursor, and the activated CMS was placed in a glove box for further use.

1.3. Fabrication of composite polymer electrolytes

Different proportions of ZIF-8 powder (0, 4, 8, 12 wt%) and LiTFSI were dissolved in NMP solvent, stirred for 2 h to obtain an evenly dispersed solution. Then, PVDF powder was dissolved in the solution and stirred continuously for 24 h to obtain a homogeneous slurry. Afterwards, the slurry was coated on a glass plate with a thickness of 500 μm. After dried for 36 h in a vacuum drying oven at 80°C, the film (140~150 μm) as peeled off from the glass plate. The final composite solid electrolytes were named as PL, 4% CPL, 8% CPL and 12% CPL, respectively.

1.4. Materials characterization

The structures of the prepared samples were investigated by X-ray diffraction (XRD, Bruker D8 Advance, Cu Kα, λ=1.541, 2θ=5°-80°). The morphology and microstructures were characterized via scanning electron microscopy (SEM, Tescan), transmission electron microscopy (TEM, FEI Tecnai F20) at 200 kV, and atomic force microscopy (AFM, Bruker multimode8). The specific surface area and pore size distribution of the materials were tested from the N_2 adsorption-desorption isotherms (Micromeritics ASAP 2020) and calculated by the Brunauer-Emmett-Teller (BET) equation. Thermo gravimetric analysis (TGA) and Differential Scanning Calorimetry (DSC) curves were measured using the Netzsch 200 F3 Synchronous thermal analyzer under N_2 flow with a heating rate of 10 ℃ min^{-1}. Fourier transform infrared spectroscopy (FTIR, Thermo Scientific Nicolet iS20) and Raman spectroscopy (DXR, Renishaw inVia Reflex, 785 nm). Tensile tests of the

composite polymer films with a size of ~15 cm×3 cm×0.015 cm were characterized on an CMT6103 with a stretching speed of 1 cm min^{-1}. The chemical composition was investigated by X-ray photoelectron spectroscopy (XPS, Thermo Scientific K-Alpha).

1.5. Electrochemical measurements

The ionic conductivity of CPE was measured by electrochemical impedance spectroscopy (EIS) of SS/electrolyte/SS blocking cell from 1 MHz to 0.1 Hz at temperature range of 28-60℃. The ionic conductivity was calculated based on the following equation (1):

$$\sigma = \frac{L}{RS}$$

where L (cm) represents the thickness of the electrolyte membrane, R (Ω) represents the electrolyte resistance, and S (cm^2) is the area of SS electrode. Activation energy (E_a) of Li-ion conducting in electrolytes can be calculated from the Arrhenius equation (2):

$$\sigma = Aexp\left(\frac{-E_a}{K_bT}\right)$$

where σ represents the ionic conductivity of the electrolyte, A represents the pre-exponential factor, K_b represents the Boltzmann constant, T is the absolute temperature. The Li-ion transference number (t_{Li^+}) was measured by direct-current (DC) polarization of Li/Li symmetric cell with a voltage polarization of 10 mV. The t_{Li^+} was calculated based on the following equation (3):

$$t_{Li^+} = \frac{I_s(\Delta V - I_0R_0)}{I_0(\Delta V - I_sR_s)}$$

where I_0 and I_s were the initial and steady-state currents, R_0 and R_s were the resistance values before and after the polarization, ΔV represent the voltage polarization applied. Electrochemical stability was tested by linear sweep voltammetry (LSV) using SS/electrolyte/Li cell from 2.5 to 6 V. Electrical conductivity of the composite electrolytes was determined by DC polarization test of 2 V conducted in the composite electrolyte-based symmetric stainless-steel battery. Equation (4) was employed to calculate the electrical conductivity.

$$\sigma_e = \frac{I_sL}{EA}$$

where I_s, L, E, A stand for the steady-state current, the thickness of the electrolyte, applied polarization potential, and surface area of the working electrode, respectively.

The Li plating/stripping cycles (The Li symmetrical cell was charged and discharged for 1 h at 28°C with a current density of 0.1 mA cm^{-2}), the critical current density (CCD) test results and battery cycling performance (Voltage range from 2.5~4.2 V, 1C=170 mA h g^{-1}, cycling at different C-rates) were obtained with a LAND battery cycler and Neware battery test system (CT-4008T-5V50Ma-164, Shenzhen, China). Typically, LFP powder, Super P, and PVDF binder was mixed at a weight ratio of 8:1:1 to obtain the electrode slurry, which was then casted onto the surface of Al foil and vacuum dried at 100℃ for 10 h. The average loading capacity of the active substance is ~1.30 mg·cm^{-2}. The $LiNi_{0.8}Co_{0.1}Mn_{0.1}O_2$ (NCM811) was prepared using the same method and it average loading capacity of the active substance is ~1.40 mg·cm^{-2}. All the cells were assembled in an Ar-filled glove box without adding any liquid electrolyte or solvent.

1.6. Density functional theory (DFT) calculations

All calculations were carried out by Perdew-Burke-Emzerhof (PBE) functional and projector augmented wave (PAW) potentials using the Vienna Ab Initio Simulation Package (VASP). [S1-3] The projector augmented wave method was adopted to describe the frozen core electrons and their interaction with the valence electrons. The cutoff energy used was 450 eV and the calculations include spin polarization. The convergence standards of energy and force were 10^{-5} eV and 0.02 eV/Å for geometry optimization. A vacuum space of 15 Å thickness was adopted to prevent non-physical interaction between periodic images in the Z-axis directions. The adsorption energy (E_b) was calculated to describe the interaction strength between the adsorbates and catalysts, and the energy variation in the adsorption process was determined according to the following equation: $E_b = E_{ads/sub} - E_{sub} - E_{ads}$, where the $E_{ads/sub}$, E_{sub} and E_{ads} are the total energies of adsorbed system, catalyst and free adsorbate.

2. Results and Discussion

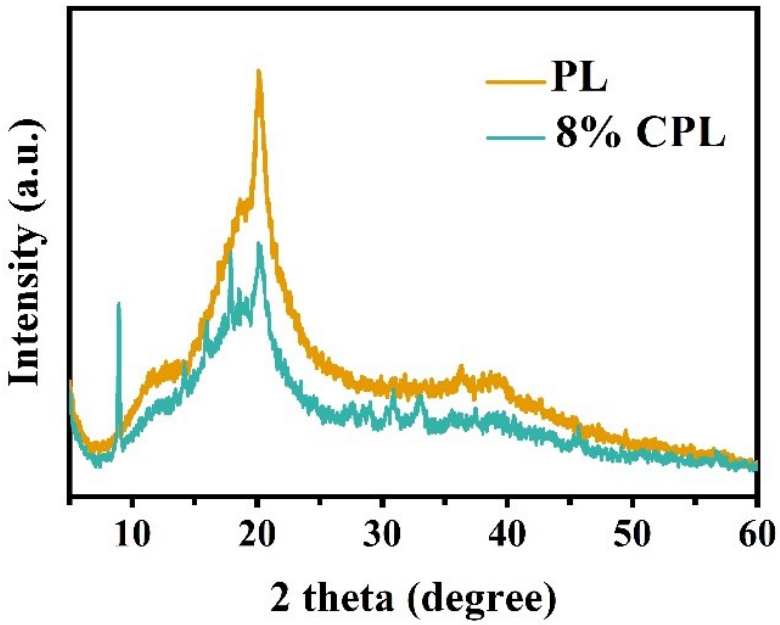

Fig. S1. XRD patterns of 8% CPL and PL electrolytes.

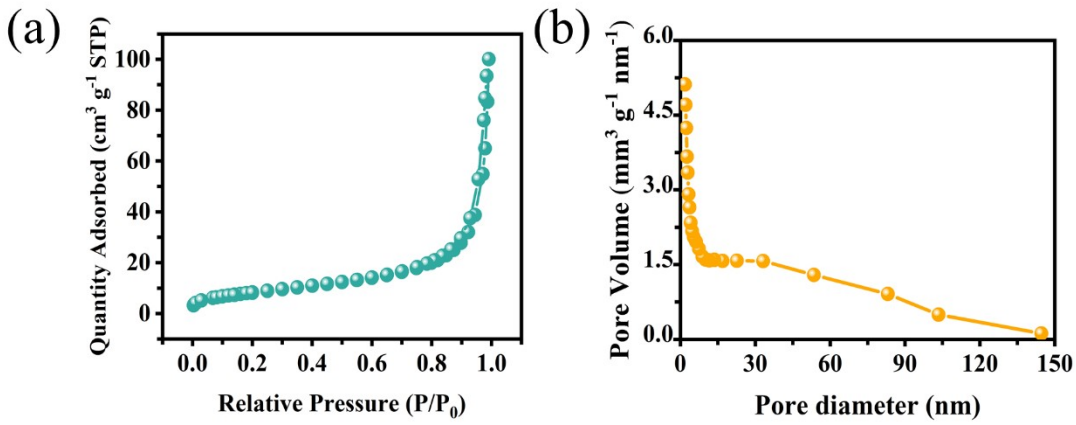

Fig. S2. (a) Nitrogen absorption/desorption isotherm of CMS and (b) pore size distribution of CMS.

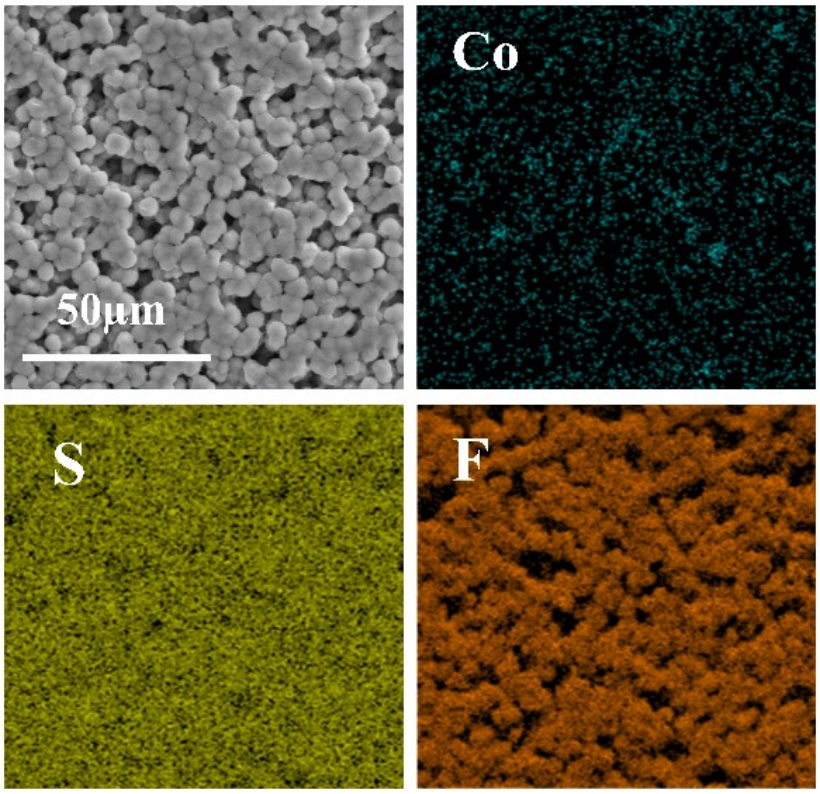

Fig. S3. EDS spectrum of the 8% CPL.

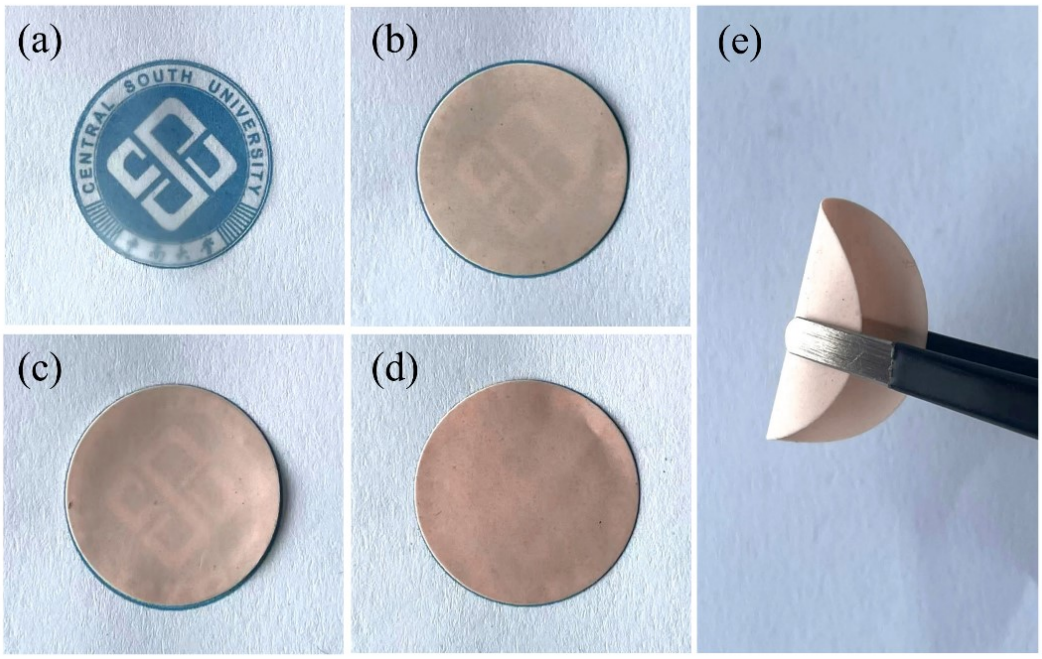

Fig. S4. (a)-(d) Photographs of PL, 4% CPL, 8% CPL, and 12% CPL electrolytes. (e) Optical photo of the 8% CPL electrolyte, showing the flexibility.

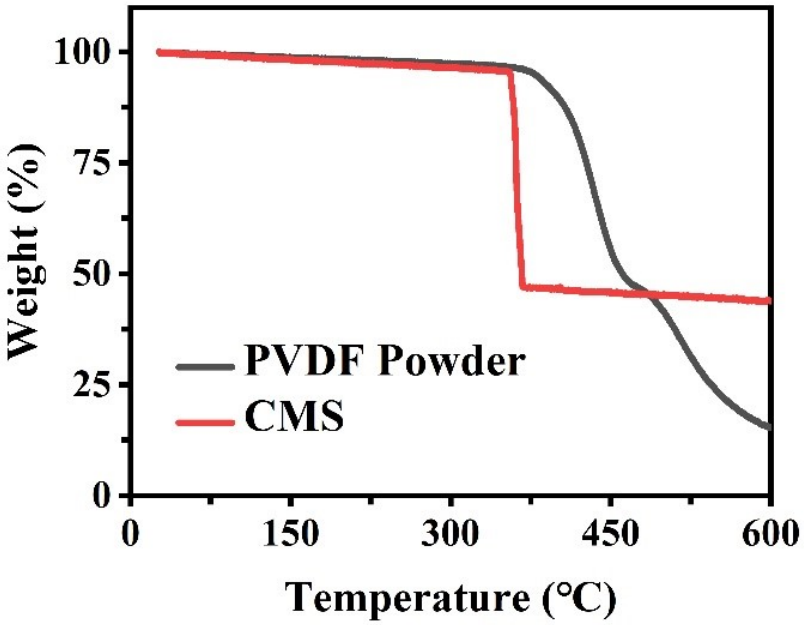

Fig. S5. TGA curves of CMS and PVDF powder.

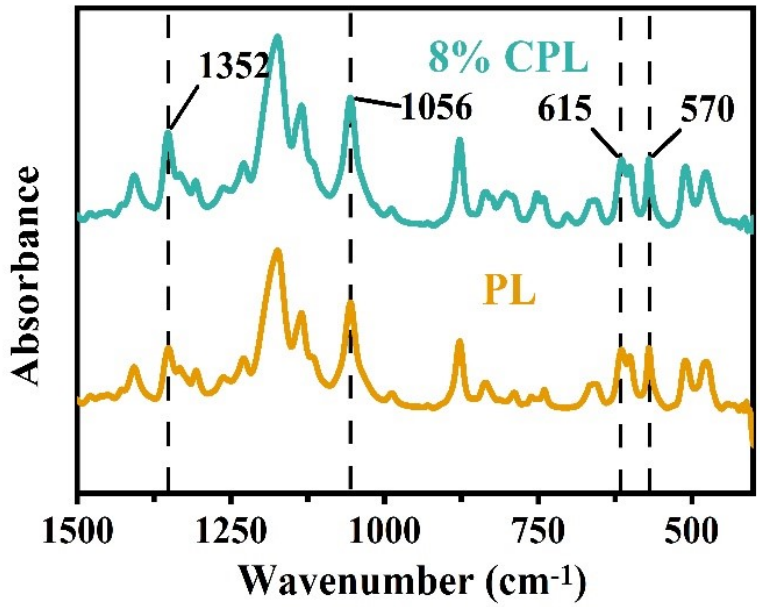

Fig. S6. FTIR curves of 8% CPL and PL electrolytes at 1500-400 cm^{-1}.

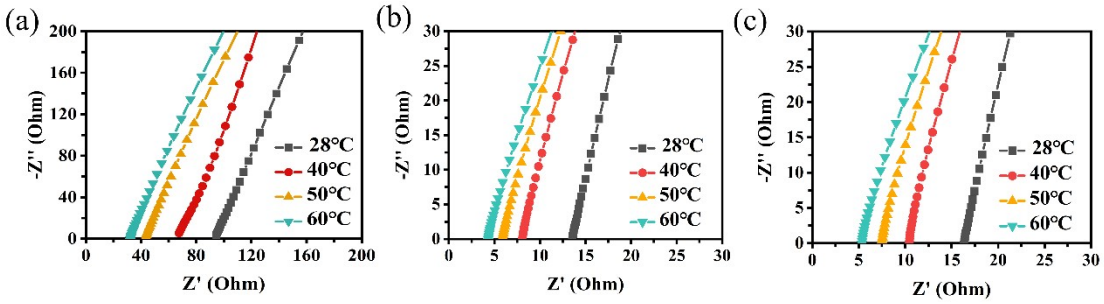

Fig. S7. EIS impedance spectra of (a) PL, (b) 4% CPL, (c) 12% CPL at various temperatures.

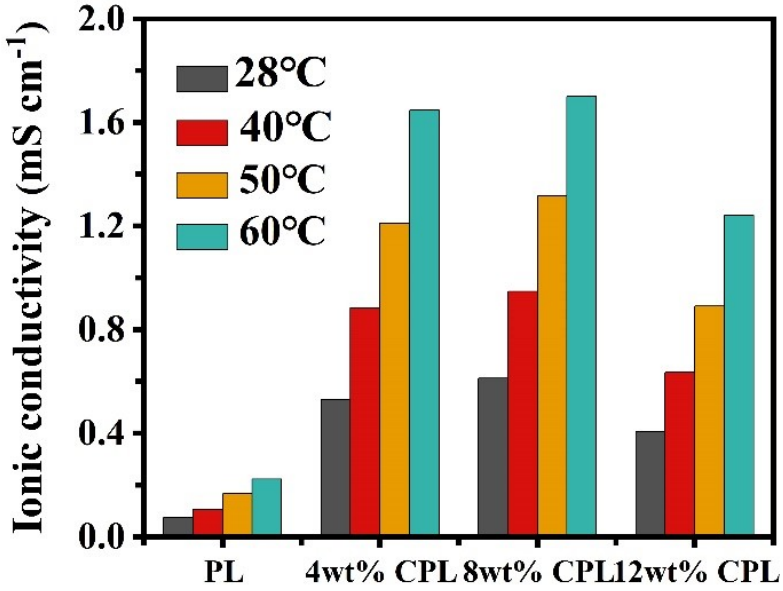

Fig. S8. Ionic conductivity of PL, 4% CPL, 8% CPL, and 12% CPL electrolytes.

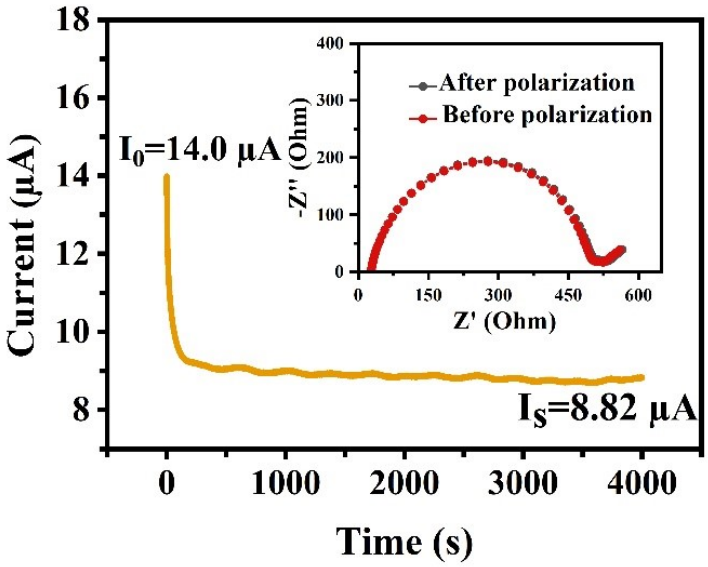

Fig. S9. Chronoamperometry curve of Li/PL/Li cell under 10 mV polarization. The inset is EIS spectra before (black) and after (red) potential polarization.

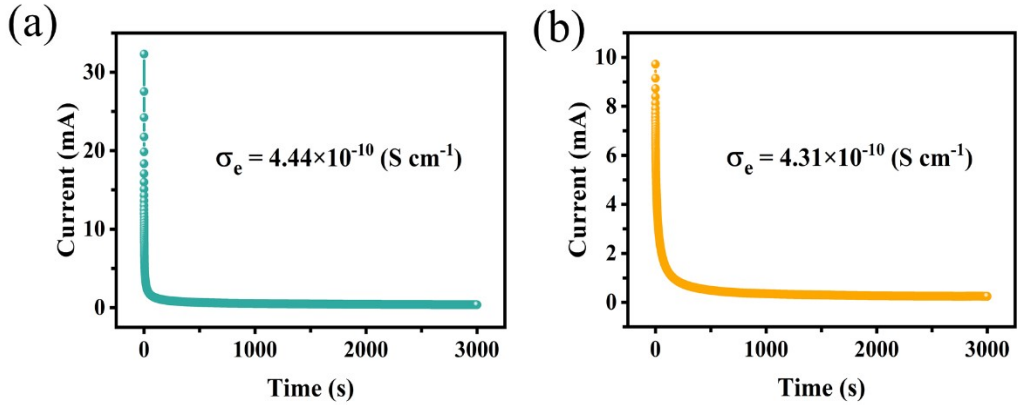

Fig. S10. DC polarization test for the (a) 8% CPL, (b) PL at 2 V.

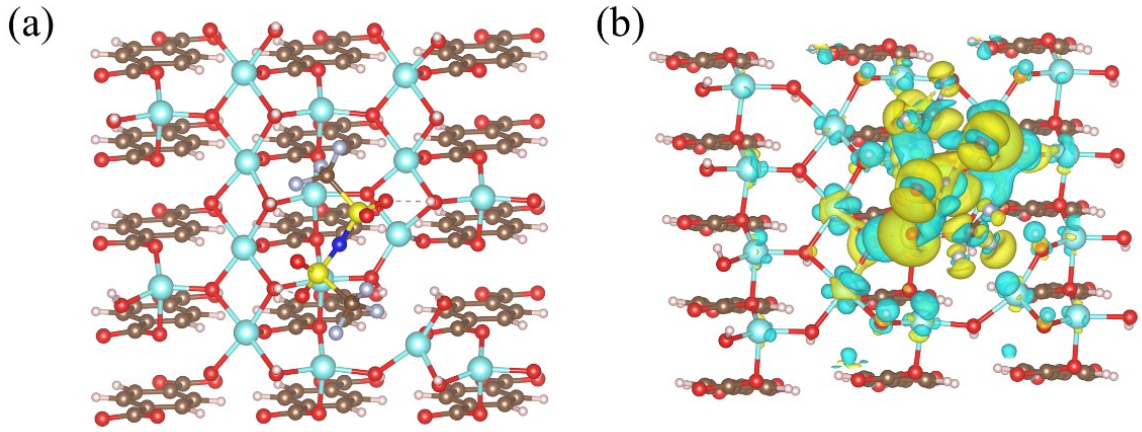

Fig. S11. (a) The atomic structures and (b) the corresponding charge density difference of TFSI-CMS.

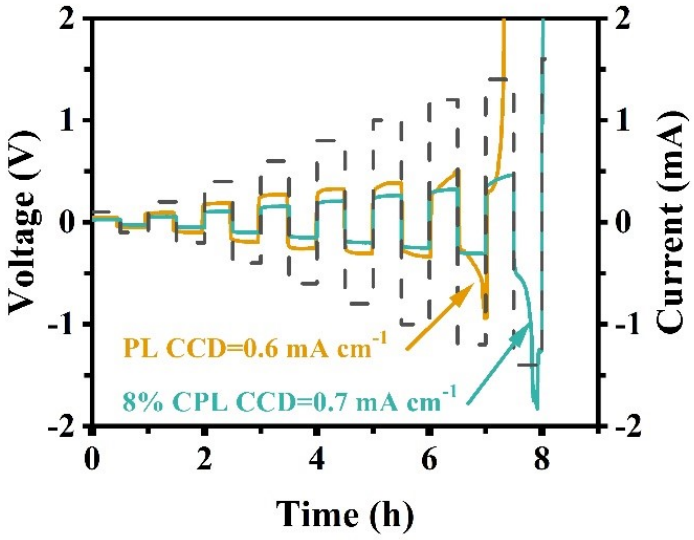

Fig. S12. Critical current density (CCD) of the Li/8% CPL/Li and Li/PL/Li cells.

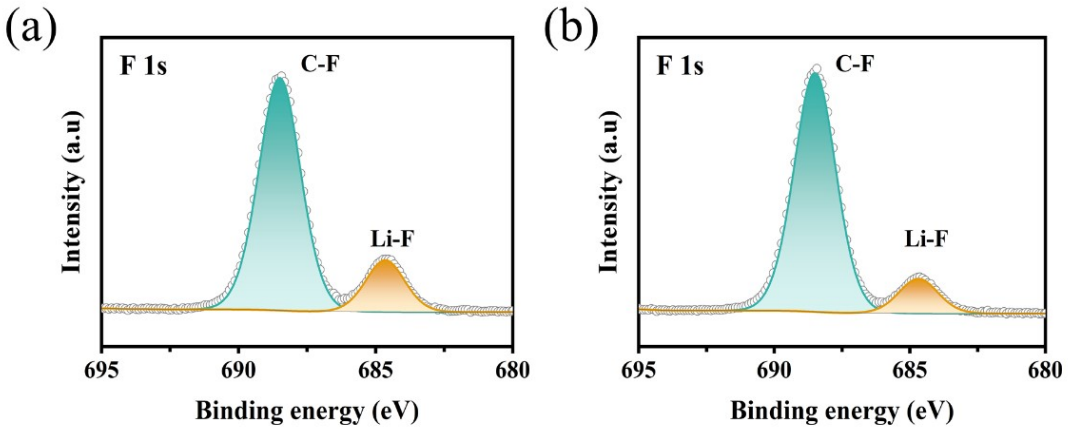

Fig. S13. Detailed XPS F1s spectrum of LFP cathode in (a) Li/8% CPL/Li and (b) Li /PL/Li after 100 cycles at 0.1 mA cm^{-2} (0.1 mA h cm^{-2}).

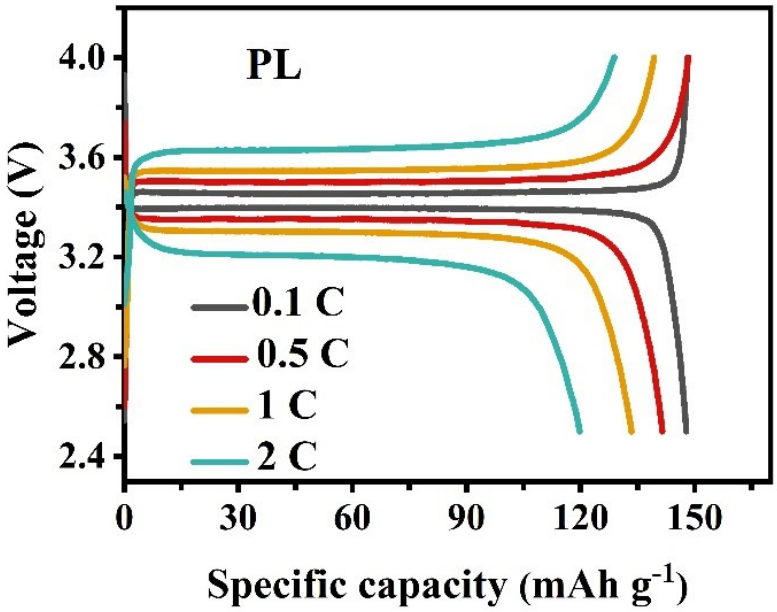

Fig. S14. Charge/discharge curves of Li/PL/LFP under different rates.

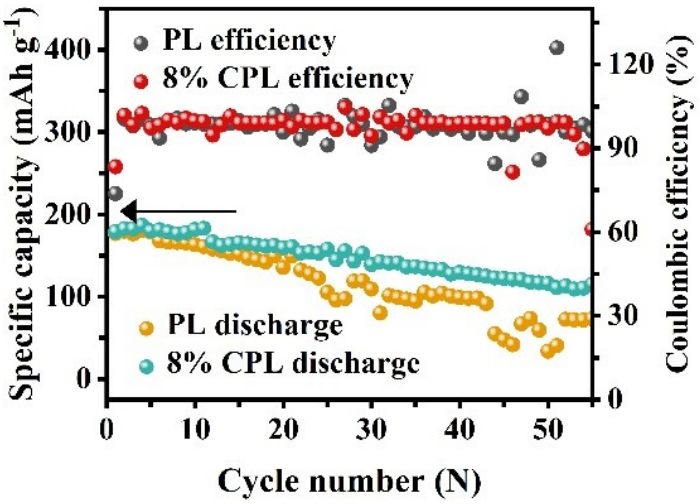

Fig. S15. Cycling performance of Li/8% CPL/NCM811 and Li/PL/NCM811 cell at 0.1 C.

Table S1. Comparison of the T_m and crystallinity of PL and 8% CPL electrolytes.

Samples	T_m (°C)	$\triangle H_m$ (J g^{-1})	X_c/%
8% CPL	142.21	11.98	11.44
PL	145.71	12.70	12.13

Table S2. FTIR peaks and assignments for LiTFSI, CMS, PL, and 8% CPL.

	Wavenumber/cm^{-1}			
Peak assignment	LiTFSI	CMS	PL	8% CPL
Asymmetric -SO_2- stretching	1325		1350	1353
C-SO_2-N bonding mode	1142		1134	1136
Stretching vibrations of OH^-		3600		3602
Asymmetric -COO- stretching		1579		1582
Symmetric -COO- stretching		1353		1353

Table S3. Comparison of ionic conductivities of PL, 4% CPL, 8% CPL, and 12% CPL electrolytes at various temperatures.

	Ionic conductivity (S cm^{-1})			
Temperature (℃)	PL	4% CPL	8% CPL	12% CPL
28	7.5759E-05	5.2919E-04	6.2635E-04	4.0698E-04
40	1.0584E-05	8.8416E-04	1.0275E-03	6.3481E-04
50	1.6614E-04	1.2150E-03	1.3938E-03	8.9044E-04
60	2.2256E-04	1.6537E-03	1.9377E-03	1.2469E-03
Thickness (cm)	0.014	0.014	0.015	0.013

References

[S1] M. Engel, M. Marsman, C. Franchini, G. Kresse, Electron-phonon interactions using the projector augmented-wave method and Wannier functions, Physical Review B. 101 (2020) 184302. https://doi.org/10.1103/PhysRevB.101.184302.

[S2] G. Kresse, J. Furthmüller, Efficient iterative schemes for ab initio total-energy calculations using a plane-wave basis set, Physical Review B. 54 (1996) 11169-11186. https://doi.org/10.1103/PhysRevB.54.11169.

[S3] J.P. Perdew, K. Burke, M. Ernzerhof, Generalized Gradient Approximation Made Simple, Phys. Rev. Lett. 77 (1996) 3865-3868. https://doi.org/10.1103/PhysRevLett.77.3865.